Antibacterial and Hypoglycemic Diterpenoids from *Salvia chamaedryoides*

Angela Bisio,*[,†] Maria De Mieri,[‡] Luigi Milella,[§] Anna M. Schito[⊥], Anita Parricchi,[†] Daniela Russo,[§] Silvana Alfei,[†] Margherita Lapillo,[∥] Tiziano Tuccinardi,[∥] Matthias Hamburger,[‡] Nunziatina De Tommasi[▽]

[†]Dipartimento di Farmacia, Università di Genova, Viale Cembrano 4, 16148 Genova, Italy

[‡]Department of Pharmaceutical Sciences, University of Basel, Klingelbergstrasse 50, 4056 Basel, Switzerland

[§]Dipartimento di Scienze, Università degli Studi della Basilicata, Viale dell'Ateneo Lucano 10, 85100, Potenza, Italy

[⊥]Dipartimento di Scienze Chirurgiche e Diagnostiche Integrate, Sezione di Microbiologia, Università di Genova, Largo Rosanna Benzi 8, 16145 Genova, Italy

[∥] Dipartimento di Farmacia, Università di Pisa, via Bonanno 6 and 33, 56126 Pisa, Italy

[▽]Dipartimento di Farmacia, Università di Salerno, Via Giovanni Paolo II 132, 84084 Salerno, Italy

*Corresponding author. Tel: +39-010-3532638; fax: +39-010-3532684. *E-mail address*: bisio@difar.unige.it

ABSTRACT: A surface extract of the aerial parts of *Salvia chamaedryoides* afforded 13 diterpenes (**1**–**13**), with seven compounds (**1**, **3**, **4**, **7**–**9**, **12**) described for the first time. The structures of the new compounds were established using 1D and 2D NMR spectroscopic methods, HRESIMS, and ECD data. The potential hypoglycemic effects of the crude extract, fractions, and pure compounds from *S. chamaedryoides* were investigated by inhibition of α-glucosidase and α-amylase enzymes. The extract and its fractions showed a moderate dose-dependent inhibition; the pure compounds exhibited differential inhibitory activity against these two enzymes. Molecular modeling studies were also performed to suggest the interaction mode of compound **3** in the α-glucosidase enzyme active site. The antimicrobial activity of the purified compounds was investigated against 26 clinical pathogens. No activity was detected for the Gram-negative species tested nor on *Candida albicans* and *C. glabrata*, while variable susceptibilities were observed using Gram-positive staphylococcal and enterococcal species.

In the course of research on bioactive terpenoids from Salvia species introduced in the Mediterranean coastal areas for both ornamental and pharmaceutical purposes,(1-3)Salvia chamaedryoides Cav. (Lamiaceae) was examined, and this was selected on the basis of a chemotaxonomic approach. S. chamaedryoides(4) is a Mexican perennial species,(5, 6) of the section Flocculosae,(6) and belongs to the same clade termed “core Calosphace”(7) of other Salvia species that have been studied previously.(8-11) From a phytochemical point of view, this clade is mainly characterized by the presence of clerodane diterpenes,(12) for which antifeedant, cytotoxic, antimicrobial, antiprotozoal, hypoglycemic, and hallucinogenic activities have been reported.(13-16) In the present investigation, the diterpenoids were characterized of a lipophilic plant surface extract of S. chamaedryoides, and these compounds were subjected to evaluations of their in vitro hypoglycemic and antimicrobial activities. The investigation of these two biological activities was performed on the basis of the following considerations. First, the isolation and identification of α-amylase and α-glucosidase inhibitors from plants are gaining interest due to the growing importance of pathologies related to these enzymes,(17, 18) and terpenoids have been reported among compounds displaying such activity.(19, 20) Second, due to the constantly increasing resistance to antibiotics(21) and the interesting results shown by several other species of Salvia,(3, 9, 22, 23) the antimicrobial properties of the isolated compounds were also tested.

RESULTS AND DISCUSSION

The dichloromethane extract of a surface mixture, obtained from the aerial parts of S. chamaedryoides, afforded seven new diterpenoids, 1, 3, 4, 7, 8, 9, and 12, along with six known diterpenes, namely, salvimicrophyllin B (2),(24) 7α-hydroxybacchotricuneatin A (5),(25) tilifodiolide (6),(26) splendidin C (10),(27) galdosol (11),(28) and rosmanol (13).(29, 30) The known diterpenoids were identified by comparison of their physical and spectroscopic data with literature values.

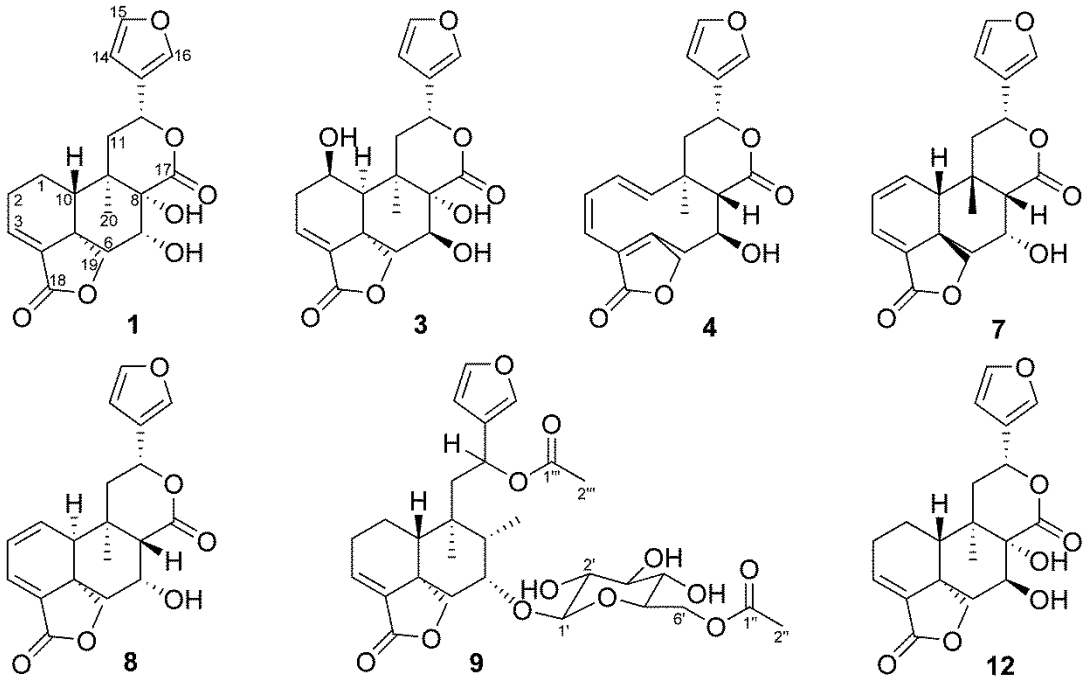

Compounds **1**, **3**, **4**, **7**, **8**, **9**, and **12** were characterized as furano-diterpenes on the basis of their spectroscopic features. The IR spectra (KBr) exhibited stretching frequencies for OH (3400–3567 cm^{-1}) and C═O (1738–1766 cm^{-1}) groups and a β-substituted furan ring (3083–3160, 1500–1510, and 870–877 cm^{-1}). The ^{1}H and ^{13}C NMR data (Tables 1–3) confirmed the presence of the furan ring [δ_C 108.4–108.9 (C-14), 143.8–144.4 (C-15), 139.7–140.6 (C-16); δ_H 6.40–6.47 (1H, br s, H-14), 7.39–7.46 (1H, br s, H-15), and 7.42–7.52 (1H, br s, H-16)] and of an 18,19-γ-lactone [δ_C 168.5–174.8 (C-18), 72.0–80.8 (C-19); δ_H 3.84–4.70, 4.36–5.30 (H_2-19)]. In addition, compounds **1**, **3**, **4**, **7**, **8**, and **12** contained a 17,12-δ-lactone [δ_C 171.3–175.3 (C-17), 64.9–72.6 (C-12); δ_H 5.33–5.98 (H-12)].

Compound 1 (HRESIMS m/z 397.1259 [M + Na]+) showed a molecular formula of C20H22O7, equating to 10 double-bond equivalents. The 13C NMR spectrum was indicative of a clerodane skeleton, as it showed 20 resonances that were attributed to one methyl, five methylenes, seven methines, and seven quaternary carbons including two carbonyl groups (Table 1).(31) A double doublet at δH 6.74 (1H, J = 7.4, 1.7 Hz) was assigned to H-3 (HMBC correlations: H-1α/C-3, H2-2/C-3, H-3/C-1, H-3/C-2, H-3/C-5, H-3/C-18) (Table 1). A secondary and a tertiary hydroxy group could be located at C-7 and C-8, respectively [δC 69.2 (C-7), 78.0 (C-8); δH 4.49 (1H, t, J = 6.7, 6.7 Hz, H-7)], as inferred from the 1D-TOCSY and COSY spectra and HMBC correlations of H2-6/C-7, H2-6/C-8, H-7/C-5, H-7/C-6, H-7/C-17, H-10/C-8, H2-11/C-8, and H3-20/C-8 (Table 1). The relative configurations of the stereocenters were inferred by ROESY correlations and analysis of 1H NMR J-

couplings. The A/B junction was deduced to be trans on the basis of the ROESY cross-peaks of H-1α/H-19pro S, H-1α/H3-20, H-2β/H-10, H-7/H-10, and H2-19/H3-20. The coupling constants of H-7 (δH 4.49, t, J = 6.7, 6.7 Hz), in conjunction with the strong dipolar coupling H-7/H-12, indicated an α-orientation for the OH-7 group (Table 1) and a twisted-boat conformation for the B ring. To confirm the position of the OH groups at C-7 and C-8, an acetonide derivative of 1 was prepared. The presence of the 1H NMR signals [δH 1.55 (3H, s) and 1.70 (3H, s)] of the two methyl groups in the acetonide (Figure S6, Supporting Information) suggested a syn relationship of the OH groups(32) and a cis fusion of rings B/C. The magnitude of the H-12 coupling constants (J11ax-12 = 12.3 and J11eq-12 = 2.4 Hz) indicated an α-equatorial orientation of the furan ring, which was confirmed by ROESY correlations of H-7/H-12 and H-10/H-12 (Figure 1). The absolute configuration of 1 was established by electronic circular dichroism (ECD). The experimental ECD spectrum showed a negative Cotton effect (CE) at 245 nm, corresponding to a weak UV absorption, and a positive CE at 216 nm, due to n → π and π → π electronic transitions, respectively, of the α,β-unsaturated γ-lactone ring. The negligible contribution of the furan ring to the ECD spectrum of 1 was corroborated by comparison of the calculated ECD spectra of 1 and its tetrahydrofuran analogue, which were superimposable (Figure 2A). The experimental ECD spectrum of 1 matched that calculated for the (5S,7R,8S,9R,10S,12R) stereoisomer (Figure 2A). Therefore, the structure of 1 was established as (5S,7R,8S,9R,10S,12R)-7,8-dihydroxycleroda-3,13(16),14-triene-17,12;18,19-diolide.

The HRESIMS (positive-mode) of 3 displayed a sodium adduct ion at m/z 413.2712 [M + Na]+, corresponding to a molecular formula of C20H22O8. On the basis of NMR spectroscopic data, the gross structure of 3 was found to be similar to that of 1, with the presence of an additional oxygenated methine at C-1 [δC 75.7 (C-1); δH 4.54 (1H, ddd, J = 8.0, 3.2, 1.3 Hz, H-1)], as confirmed by the COSY spectrum, and by HMBC correlations of H-1/C-3, H-1/C-5, H-1/C-9, H-2β/C-1, and H-3/C-1 (Table 1). The ROESY correlations of H-10/H-19(pro S) and H-10/H3-20 suggested the presence of a cis-decalin ring. A 3J H-1/H-10 coupling constant of 3.2 Hz and a ROESY cross-peak of H-1/H-10 supported the β-orientation of OH-1. The absence of the methyl signals in the 1H NMR spectrum of the acetonide derivative of 3 indicated the two OH groups at C-7 and C-8 to be anti.(32) The coupling constants of H-7 [δH 4.41 (1H, dd, J7–6ax = 8.0 and J7–6eq = 1.0 Hz)] (Table 1) were consistent with a β-equatorial orientation for OH-7 and a twisted boat conformation of the B ring. Taken together, the data confirmed the α-orientation of OH-8 and, consequently, the B/C cis ring fusion. The magnitude of the H-12 coupling constants (J11ax-12 = 12.0 and J11eq-12 = 3.7 Hz) (Table 1) and the ROESY cross-peak observed for H-1/H-12 (Figure 1) were in agreement with an α-equatorial orientation of the furan

ring. The experimental ECD spectrum of 3 showed a close similarity to that of 1 (Figure 2B), thereby suggesting the same S absolute configuration at C-5. Thus, compound 3 was established as (1R,5S,7S,8S,9R,10R,12R)-1,7,8-trihydroxycleroda-3,13(16),14-triene-17,12;18,19-diolide.

Compound 4 gave a molecular formula of C20H20O6, as deduced from its HRESIMS (m/z 379.1005 [M + Na]+), indicating 11 degrees of unsaturation. The NMR data of 4 were indicative of a 5,10-seco-neo-clerodane skeleton similar to that of salvimicrophyllin A,(24) but with an additional secondary OH group at C-7 [δC 71.0 (C-7); δH 4.64 (1H, ddd, J = 13.2, 5.3, 2.0 Hz, H-7)]. This was confirmed using the COSY spectrum and from HMBC correlations between H2-6/C-7, H-7/C-5, H-7/C-6, H-7/C-8, and H-7/C-9 (Table 2). The magnitude of the J coupling of H-7 and H-8 (J7–8 = 2.0 Hz) and their ROESY correlation inferred their cofacial orientation. ROESY cross-peaks of H-8/H-10 and H-11α/H3-20 indicated the cofacial orientation of these protons and a trans ring junction. As found for salvimicrofillin A, the H-12 coupling constants (J11ax-12 = 12.3 and J11eq-12 = 3.0 Hz) (Table 2) indicated an equatorial orientation of the furan ring, which together with the ROESY correlation H-8/H-12 corroborated the β-orientation of these protons. The experimental ECD spectrum of 4 matched that calculated for the (7R,8S,9R,12R) stereoisomer (Figure 2C). On the basis of these results, compound 4 was established as (7R,8S,9R,12R)-7-hydroxy-5,10-seco-neo-cleroda-1(10),2,4,13(16),14-pentaene-17,12;18,19-diolide.

Compound 7 exhibited a molecular formula of C20H20O6 (HRESIMS m/z 379.2964 [M + Na]+), equating to 11 degrees of unsaturation. The UV, IR, and NMR spectroscopic data indicated a close similarity of its gross structure with that of salvimicrophyllin C,(24) but with an additional oxygenated methine at C-7 [δC 63.3 (C-7); δH 4.69 (1H, ddd, J = 9.0, 8.0, 3.9 Hz, H-7)] (Table 1), as confirmed by the COSY spectrum and by the HMBC correlations of H-6/C-7, H-7/C-6, and H-7/C-9 (Table 1). The chemical shift of CH3-20 (δC 28.6) (Table 1) suggested a cis-ring junction of the decalin system.(33) Selective 1D-ROESY experiments were performed to assign the relative configuration (Figure S19 Supporting Information). Upon irradiation of H-10, ROE correlations were observed with the H-8, H2-19, and H-11β signals, while selective irradiation of H-12 enhanced H-8, H-11β, and H-10 and irradiation of H-7 enhanced H-8, H-19pro R, and H-6β. These data supported the cofacial orientation of H-7, H-8, H-10, and H-12. On the other hand, selective irradiation of H3-20 strongly enhanced H-1, H-6α (axial), and H-11α (axial) and thereby were consistent with the α-orientation of H3-20 and a B/C trans ring junction. The 1H NMR J couplings of H-7 δH 4.69 (1H, ddd, J = 9.0, 8.0, 3.9 Hz) agreed with the dihedral angles found in the optimized structure (Figure 1). In the experimental ECD spectrum of 7 (Figure 2D) the conjugated π system showed consecutive negative and positive CEs at 256 and

305 nm, respectively. The calculated ECD spectrum for the ent-(5S,7S,8R,9S,10S,12S) stereoisomer (Figure 2D) was the mirror image of the experimental data and thereby indicated that 7 belongs to the normal clerodane series. This configurational assignment was supported by the close similarity of the ECD spectra of 7 and salvimicrophillyn C.(24) On the basis of the above findings, compound 7 was assigned as (5R,7R,8S,9R,10R,12R)-7-hydroxycleroda-1,3,13(16),14-tetraene-17,12;18,19-diolide.

The spectroscopic data of compound 8 (HRESIMS m/z 379.1027 [M + Na]+) indicated this compound to have the same molecular formula and planar structure as 7. Differences in the 1H and 13C NMR spectra (Table 3) suggested that these compounds are diastereoisomers. Diagnostic ROESY correlations of H-10/H-19pro S, H-10/H3-20, and H2-19/H3-20 indicated that these groups are cofacial and supported the cis fusion of the decalin ring. On the other hand, the ROESY correlation between H-8 and H-12, as well as the values of the H-12 1H NMR coupling constants (J11ax-12 = 12.5 and J11eq-12 = 4.3 Hz) (Table 3), indicated an α-equatorial orientation of the furan ring and a trans-junction between the B/C rings. The α-orientation of OH-7 was deduced from the J coupling of H-7 and H-8 (J7–8 = 2.3 Hz) and corroborated by the ROESY correlation of H-7/H-8. The experimental ECD spectrum of 8 showed a very good match with that calculated for the ent-(5S,7R,8S,9R,10S,12R) stereoisomer (Figure 2E). Thus, compound 8 was assigned as (5S,7R,8S,9R,10S,12R)-7-hydroxycleroda-1,3,13(16),14-tetraene-17,12;18,19-diolide.

For compound 9, a molecular formula of C30H40O12 was deduced from the HRESIMS (m/z 615.2393 [M + Na]+). The 1H and 13C NMR spectra (Table 2) showed resonances characteristic of a clerodane diterpene with a hexose unit and an acetyl group. This was confirmed by the MS fragmentation pattern showing fragment ions at m/z 555 [(M – CH3COOH) + Na]+ and m/z 333 [(M – C8H14O7) + Na]+, due to the loss of hexose and acetyl groups. The NMR data of the aglycone were closely compatible with those of salvisplendin C,(34) the 12-acetoxy derivative of 7α,12α-dihydroxyhautriwaic acid-19-lactone.(35) The assignment of the hexose residue was achieved by COSY and HMBC experiments (Table 2). Five oxygenated protons with all-trans diaxial interactions showed the typical spin system of a β-glucopyranoside unit. The acetyl group was attached at C-6′, as confirmed by HMBC correlations of H-6′/C-1″ and H-2″/C-6′. The coupling constant of the anomeric proton [δH 4.32 (1H, d, J = 7.9 Hz, H-1′)] indicated a β configuration of the glucosyl moiety.(36) With the aid of an HPLC method described by Tanaka et al.(37) the glucose unit was assigned to the d-series. The attachment of the sugar moiety at C-7 of the aglycone was established by an HMBC correlation from the anomeric proton H-1′ to C-7 and a downfield shift of C-7 (δC 79.1) as compared to salvispendin C. According to the ROESY data, the relative configuration of 9 was the same as in

salvisplendin C.(34) The ECD spectrum of 9 (Figure 2F), similar to that of 1, showed consecutive negative and positive Cotton effects at 216 and 245 nm due to π → π and n → π electronic transitions, respectively, of the α,β-unsaturated γ-lactone ring. The configuration of the tricyclic scaffold of 9 was established by comparison with the calculated ECD spectrum. However, the configuration at C-12 could not be established, since the calculated ECD spectra for the epimers at C-12 did not differ significantly. Therefore, compound 9 was characterized as (5S,7R,8S,9R,10R)-7-(6-O-acetyl-β-d-glucopyranosyl)hydroxy-12-O-acetylcleroda-3,13(16),14-triene-17,12;18,19-diolide.

Compound 12 gave the same molecular formula as (HRESIMS m/z 397.2813 [M + Na]+) and similar NMR data to those of 1 (Table 3). Differences in their NMR spectra, particularly for H2-6 (1: δH 2.04 and 2.08 vs 12: δH 1.83 and 2.31), H-7 (1: δH 4.49, t, J = 6.7, 6.7 Hz vs 12: 4.34, ddd, J = 4.5, 2.2, 2.2 Hz), H-10 (1: δH 2.01 vs 12: 2.52, dd, J = 12.8, 1.8 Hz), H2-11 (1: 1.98 and 2.15 vs 12: 1.81 and 2.34), H-12 (1: 5.53, dd, J = 12.3, 2.4 Hz vs 12: 5.98, t, J = 8.3, 8.3 Hz), and H3-20 (1: 0.98, s vs 12: 1.20, s), and in optical rotation [1: −106.7 (c 0.30, CH3OH) vs 12: −26.9 (c 0.51, CH3OH)] suggested a different configuration. The relative configuration of 12 was established by analysis of J couplings and ROESY correlations. Cross-peaks observed for H-10/H-6β, H-10/H-1β, and H2-19/H3-20 indicated their cofacial arrangement and a trans junction of the A/B rings. Likewise, the correlations of H-14/H3-20 suggested an α-oriented furan ring. The compound did not form an acetonide when treated with 2,2-dimethoxypropane and a catalytic amount of p-toluenesulfonic acid. Thus, the two OH groups at C-7 and C-8 were in an anti position. At this point, two diastereomers at carbons C-7 and C-8, namely, 7S,8S and 7R,8R, were conceivable, implying a cis- or trans-junction of the B/C rings, respectively. Different 1H NMR J couplings of H-12 in compounds 1 and 12 (1: δH 5.53, dd, J = 12.3, 2.4 Hz vs 12: 5.98, t, J = 8.3, 8.3 Hz) suggested a different orientation of the C ring. Then, the calculated ECD spectra were compared for the 7R,8R and 7S,8S stereoisomers of 12 with the experimental spectrum (Figure 3). Although very similar, the ECD spectrum of the 7R,8R stereoisomer showed a closer match to the experimental one. The 7R,8R configuration was corroborated by the J couplings of H-7 and H-12 that agreed with the dihedral angles found in the optimized structure, where the C ring adopted a twisted boat conformation (Figure 3B). Thus, 12 was established as (5S,7R,8R,9R,10S,12R)-7,8-dihydroxycleroda-3,13(16),14-triene-17,12;18,19-diolide.

The isolated compounds were tested for α-glucosidase and α-amylase activity, as used as a pharmacological approach directed to decrease postprandial hyperglycemia by delaying the absorption of glucose.(38) Acarbose, currently used in hyperglycemia treatment, was employed as the positive control. The plant dichloromethane extract inhibited α-glucosidase and α-amylase, with IC50 values of

55.8 ± 6.1 and 121 ± 12 μg/mL, respectively. The active fractions showed a dose-dependent inhibition with both enzymes (Figure S35, Supporting Information), and the results were expressed as IC50 values (Table S1, Supporting Information). The inhibitory activities for α-amylase of fractions IV–VI were less potent than for acarbose (IC50 66.5 ± 2.5 μg/mL), and the most active fraction (V) showed an IC50 of 255 ± 19 μg/mL. In contrast, the inhibition of α-glucosidase was more potent than with acarbose (IC50 484 ± 30 μg/mL). Fraction V was the most active, with an IC50 of 25.9 ± 1.5 μg/mL. The α-amylase inhibition values of the pure compounds were lower than for acarbose and were in line with the activity of fractions, but compound 8 demonstrated a comparable value (IC50 53.5 ± 2.5 μg/mL). In the α-glucosidase inhibition assay, compounds 1, 3, 6, and 11 were more active than acarbose (IC50 484.2 ± 2.5 μg/mL). Among these, compound 3 was the most active, with an IC50 of 238.1 ± 4.5 and 113.2 ± 2.5 μg/mL in the α-amylase and α-glucosidase inhibition assays, respectively (Figure 4).

The binding interactions were analyzed of compound 3 and α-1,4-glucosidase (EC 3.2.1.20) by a molecular docking study and by molecular dynamics (MD) simulations. Since a crystal structure of the enzyme is not available, a recently published homology model of α-1,4-glucosidase(39) was used instead. A robust AUTODOCK procedure(40) was employed to dock compound 3 into the catalytic site of the α-1,4-glucosidase model. The docking calculation generated 200 different docking poses that were clustered with a root-mean-square deviation (RMSD) tolerance of 2.0 Å. By using this threshold, a single cluster containing all 200 poses was obtained, suggesting only one probable binding mode for the compound. The predicted docking pose was then subjected to an MD simulation to assess the stability of the suggested binding mode. The applied MD protocol was the same as previously tested by using the X-ray complex of oligo-1,6-glucosidase with maltose.(39, 41) The α-glucosidase–3 complex was subjected to a total of 50 ns of MD simulation. The system reached an equilibrium after only 200 ps, and the total energy remained constant for the remaining 49.8 ns of simulation (Figure S36, Supporting Information). The RMSD analysis of the position of the ligand with respect to the input docking pose calculated for 3 highlighted that it only slightly shifted its binding disposition, with an average RMSD value of 2.1 Å. Figure 5 shows the minimized average structure of the α-1,4-glucosidase model complexed with compound 3 obtained from all 50 ns of the MD simulation. The hydroxy group at C-8 of this diterpene formed a hydrogen bond with the catalytic residue D349 and, by means of a water molecule, gave an additional water-bridge interaction with R312. Furthermore, the neighboring hydroxy group at C-7 was connected to R312, D408, and the backbone of F157 through two water molecules. The oxygen atom of the furan ring was involved in a hydrogen bond network

with R212, H348, and R433 by means of a water molecule. Moreover, the carbonylic portion at C-18 of the 18,19-γ-lactone showed a water-mediated hydrogen bond with H245, and the diterpene backbone interacted with a hydrophobic surface mainly defined by F157, F158, F177, T215, and L218. The binding mode was thus similar to that previously suggested for an eriodictyol derivative showing good inhibition of α-1,4-glucosidase.(39)

The plant extract was also tested for antimicrobial activity against 26 clinical strains, including several isolates resistant or multidrug resistant to classical antibacterial drugs. Minimal inhibitory concentrations (MICs) are shown in Table S2, Supporting Information. All Gram-negative and Candida species tested were not inhibited by the extract (data not shown). Among the Gram-positive species, enterococci were particularly susceptible, with MIC values ranging from 2 to 4 μg/mL against E. faecium and E. faecalis. In contrast, MIC values against staphylococci were >128 μg/mL. The antibacterial activity of fractions I–VII was also investigated. Fractions I and II were inactive against all pathogens tested (data not shown), while the other fractions were active against staphylococci and enterococci (Table S2, Supporting Information). MIC values (Table 4) of compounds 1, 4, 6, 7, 10, 11, and 12 indicated that only enterococci, in particular E. faecium, were susceptible.

Previous studies have reported the in vitro inhibition of α-amylase and α-glucosidase of extracts and pure compounds (mainly flavonoids) from different species of Salvia, even if a correlation between the activity of the extracts and the isolated pure compounds was not fully demonstrated. Thus, it can be hypothesized that the enzymatic inhibitory capacity of Salvia is due to the presence of other secondary metabolites.(42, 43) To the best of our knowledge this is the first report on the α-amylase and α-glucosidase inhibition of S. chamaedryoides. Molecular modeling studies with the most active compound 3 suggested that this diterpenoid binds via an interaction with the catalytic residue D349 and, via water molecules, interacts also with other surrounding polar amino acids.

EXPERIMENTAL SECTION

General experimental procedures. Optical rotations, LC, TLC, MPLC, analytical and semipreparative HPLC, UV, IR, NMR, and MS experiments were obtained as previously described.(9, 22, 23) ECD spectra were measured in CH3OH on a Chirascan CD spectrometer (Leatherhead, Surrey, United Kingdom) and were analyzed with Pro-Data V2.4 software. All spectrophotometric measurements were done on a SPECTROstarNano UV/vis spectrophotometer (BMG Labtech, Ortenberg, Germany) by using 90 six-well microplates. Reactions were performed in triplicate. Sodium phosphate, sodium chloride, potassium sodium tartrate tetrahydrate, 3,5-dinitrosalicylic acid, sodium

hydroxide, α-amylase from hog pancreas, starch, α-glucosidase from Saccharomyces cerevisiae, potassium phosphate monobasic, 4-nitrophenyl α-d-glucopyranoside, acarbose, and dimethyl sulfoxide were acquired from Sigma-Aldrich (Milan, Italy).

Plant material. The fresh aerial parts of Salvia chamedryoides(4) were obtained from the Centro Regionale di Sperimentazione ed Assistenza Agricola (Albenga, Italy). The plant material was identified by Dr. Gemma Bramley, and a voucher specimen is deposited at the Kew Herbarium (K) (Kew, Richmond, Surrey, UK) (voucher label: Interreg III Alcotra Progetto No. 074 "Sviluppo a Scopi Commerciali delle Potenzialità del Genere Salvia L."; verified by G.L.C. Bramley 25/09/2006, No. 13).

Extraction and isolation. Freshly harvested aerial parts (1.8 kg) of S. chamaedryoides were immersed in CH2Cl2 for 20 s. After filtration, the solvent was removed under reduced pressure to afford 14 g of dry residue. The extract was fractionated on Sephadex LH-20 (1 g portions; 63 × 2.5 cm; CHCl3–CH3OH (7:3) as an eluent; analytical TLC control) to afford seven pooled fractions, namely, fraction I (from 0 to 200 mL; 0.57 g) containing waxy compounds, fraction II (from 200 to 220 mL; 0.64 g), fraction III (from 220 to 240 mL; 4.55 g), fraction IV (from 240 to 260 mL; 5.26 g), fraction V (from 260 to 280 mL; 1.16 g), fraction VI (from 280 to 360 mL; 0.44 g), and fraction VII (from 360 to 400 mL; 0.49 g).

Fraction II was chromatographed on a silica gel column (35 × 1 cm; analytical TLC control) eluted with mixtures of n-hexane–CHCl3–CH3OH (from 50:50:0 to 0:0:100, 3.04 L) to afford 21 fractions (1–21). Fraction 9 (36.8 mg) (eluted with CHCl3 35:65, from 1.56 to 1.64 L) was further purified by semipreparative RP-HPLC [Symmetry Prep C18, 7.8 × 300 mm i.d., 7 μm particle size (Waters Corporation, Milford, MA, USA), eluents A: H2O, B: CH3OH, gradient: B 5% at time 0, B 100% at time 60 min, B 100% at time 70 min], to obtain 1 (8.3 mg).

Fraction III was chromatographed on a silica gel column (50 × 4 cm; analytical TLC control) eluted with n-hexane–CHCl3–CH3OH (from 25:75:0 to 0:90:10, 22.95 L), to afford 47 fractions (1i–47i). Fraction 16i (49.8 mg) (eluted with n-hexane–CHCl3, 10:90, from 9.8 to 10.2 L) was further purified by semipreparative RP-HPLC [μBondapack C18, 7.8 × 300 mm i.d., 10 μm particle size (Waters), isocratic conditions: eluent CH3OH–H2O, 70:30], to obtain 2 (4.7 mg). Fraction 17i (20.5 mg) (eluted with n-hexane–CHCl3, 10:90, from 10.2 to 10.6 L) was further purified by semipreparative RP-HPLC [μBondapack C18, 7.8 × 300 mm i.d., 10 μm particle size (Waters), isocratic conditions: eluent CH3OH–H2O, 70:30], to afford 3 (2.9 mg) and 4 (3.4 mg). Fraction 18i (20.2 mg) (eluted with CHCl3, from 10.6 to 10.9 L) was further purified by semipreparative RP-HPLC [Symmetry Prep C18, 7.8 ×

300 mm i.d., 7 μm particle size (Waters), eluents A: H2O, B: CH3OH, gradient: B 5% at time 0, B 100% at time 60 min, B 100% at time 85 min], to yield 5 (3.4 mg).

Fraction IV was chromatographed on a silica gel column (65 × 4 cm; analytical TLC control) eluted with mixtures of n-hexane–CHCl3–CH3OH (from 25:75:0 to 0:0:100, 21.9 L) to afford 63 fractions (1–63ii). Fraction 17ii (54.3 mg) (eluted with CHCl3, from 0.4 to 0.5 L) was purified by semipreparative RP-HPLC [μBondapack C18, 7.8 × 300 mm i.d., 10 μm particle size (Waters), isocratic conditions: eluent CH3OH–H2O, 70:30], to afford 6 (5.2 mg). Fraction 25ii (58.5 mg) (eluted with CHCl3, from 1.2 to 1.4 L) was further purified by semipreparative RP-HPLC [Symmetry Prep C18, 7.8 × 300 mm i.d., 7 μm particle size (Waters), eluents A: H2O, B: CH3OH, gradient: B 5% at time 0, B 100% at time 60 min, B 100% at time 85 min], to afford compounds 7 (3.5 mg) and 8 (4.2 mg).

Fraction V was separated on a silica gel column (35 × 1 cm; analytical TLC control) eluting with mixtures of n-hexane–CHCl3–CH3OH (from 35:65:0 to 0:0:100, 2.2 L) to afford 11 fractions (1–11iii). Fraction 8iii (24.9 mg) (eluted with CHCl3, from 1.2 to 1.4 L) was further purified by semipreparative RP-HPLC [X-Bridge RP18, 10.0 × 250 mm i.d., 5 μm particle size (Waters), eluents A: H2O, B: CH3OH, gradient: 5% to 100% B in 36 min, 100% B until 60 min], to obtain 9 (3.8 mg). Fraction 9iii (84.2 mg) (eluted with CHCl3, from 1.4 to 1.5 L) was further purified by semipreparative RP-HPLC [μBondapack C18, 7.8 × 300 mm i.d., 10 μm particle size (Waters), isocratic conditions, CH3OH–H2O, 70:30] to yield 10 (3.6 mg) and 11 (2.4 mg).

Fraction VI was chromatographed on a silica gel column (35 × 1 cm; analytical TLC control) eluted with mixtures of CHCl3–CH3OH (from 100:0 to 0:100, 1.4 L) to afford eight fractions (1–8iv). Fraction 4iv (35.2 mg) (eluted with CHCl3–CH3OH, 95:5, from 120 to 160 mL) was further purified by semipreparative RP-HPLC [μBondapack C18, 7.8 × 300 mm i.d., 10 μm particle size (Waters), isocratic conditions, CH3OH–H2O, 70:30] to yield 12 (8.3 mg) and 13 (3.4 mg).

Compound **1:** Amorphous solid; $[\alpha]_D^{25}$ -107 (*c* 0.3, CH_3OH); UV/vis λ_{max} (CH_3OH) nm (log ε) 208 (4.10); ECD (CH_3OH, *c* 0.7 mM, 0.1 cm); Δε +2.8 (216 nm), -4.5 (245 nm); IR (KBr) ν_{max} (cm^{-1}) 3446, 3149, 2936, 2861, 1766, 1743, 1661, 1506, 1452, 1366, 1242, 1197, 1168, 1106, 1021, 875, 791, 775, 744, 602; ^1H NMR and ^{13}C NMR data, see Tables 1 and 2; HRESIMS (positive ion mode) *m/z* 397.1259 $[M+Na]^+$ (calcd. for $C_{20}H_{22}O_7Na$: 397.1263); ESI-MS^2 *m/z* (rel.int.) 397 $[M+Na]^+$, 379 $[(M-H_2O)+Na]^+$ (75).

Compound **3**: Amorphous solid; $[\alpha]_D^{25}$ -65 (*c* 0.1, CH_3OH); UV/vis λ_{max} (CH_3OH) nm (log ε) 207 (3.69); ECD (CH_3OH, *c* 0.3 mM, 0.1 cm); Δε +11.5 (205 nm), -6.5 (244 nm); IR (KBr) ν_{max} (cm^{-1})

3400, 3329, 3160, 2954, 2850, 2341, 1738, 1627, 1510, 1463, 1456, 1376, 1311, 1259, 1154, 1120, 1082, 1031, 870; ^{1}H NMR and ^{13}C NMR data, see Tables 1 and 2; HRESIMS (positive ion mode) *m/z* 413.2712 $[M+Na]^+$ (calcd. for $C_{20}H_{22}O_8Na$: 413.1212); ESI-MS^2 *m/z* (rel.int.) 413 $[M+Na]^+$, 395 $[(M-H_2O)+Na]^+$ (75), 351 $[(M-H_2O-CO_2)+Na]^+$(40).

Compound **4**: Amorphous solid; $[\alpha]_D^{25}$ -75 (*c* 0.04, CH_3OH); UV/vis λ_{max} (CH_3OH) nm (log ε) 211 (4.15), 295 (3.39); ECD (CH_3OH, *c* 0.6 mM, 0.1 cm); $\Delta\varepsilon$ +22.4 (214 nm), -4.9 (283 nm); IR (KBr) ν_{max} (cm^{-1}) 3567, 3141, 2999, 2970, 2934, 2896, 1751, 1710, 1643, 1500, 1441, 1375, 1321, 1268, 1204, 1158, 1123, 1062, 1033, 1005, 875, 859, 788, 736, 705, 601; ^{1}H NMR and ^{13}C NMR data, see Tables 1 and 2; HRESIMS (positive ion mode) *m/z* 379.1005 $[M+Na]^+$ (calcd. for $C_{20}H_{20}O_6Na$: 379.1158); ESI-MS^2 *m/z* (rel.int.) 379 $[M+Na]^+$, 361 $[(M-H_2O)+Na]^+$ (97), 335 $[(M-CO_2)+Na]^+$ (58).

Compound **7**: Amorphous solid; $[\alpha]_D^{25}$ +21 (*c* 0.1, CH_3OH); UV/vis λ_{max} (CH_3OH) nm (log ε) 206 (3.99), 300 (3.54); ECD (CH_3OH, *c* 0.4 mM, 0.1 cm); $\Delta\varepsilon$ -6.4 (222 nm, *sh*), -11.9 (256 nm), +22.4 (305 nm); IR (KBr) ν_{max} (cm^{-1}) 3495, 3133, 2928, 2853, 1746, 1674, 1583, 1503, 1466, 1400, 1369, 1299, 1260, 1216, 1188, 1131, 1051, 1024, 953 874, 838, 697; ^{1}H NMR and ^{13}C NMR data, see Tables 1 and 2; HRESIMS (positive ion mode) *m/z* 379.1264 $[M+Na]^+$ (calcd. for $C_{20}H_{20}O_6Na$: 379.1158); ESI-MS^2 *m/z* (rel.int.) 379 $[M+Na]^+$, 361 $[(M-H_2O)+Na]^+$ (20).

Compound **8**: Amorphous solid; $[\alpha]_D^{25}$ -104 (*c* 0.2, CH_3OH); UV/vis λ_{max} (CH_3OH) nm (log ε) 208 (3.33),-341 (2.65); ECD (CH_3OH, *c* 0.3 mM, 0.1 cm); $\Delta\varepsilon$ +1.8 (212 nm), -0.9 (225 nm, *sh*), -4.7 (245 nm), +0.9 (265 nm), -0.14 (275 nm, *sh*), +6.0 (295 nm), -5.0 (320 nm); IR (KBr) ν_{max} (cm^{-1}) 3432, 3100, 2926, 2871, 2846, 1761, 1649, 1606, 1500, 1459, 1440, 1365, 1296, 1268, 1206, 1178, 1121, 1018, 960, 877, 838, 764, 688; ^{1}H NMR and ^{13}C NMR data, see Tables 1 and 2; HRESIMS (positive ion mode) *m/z* 379.1027 $[M+Na]^+$ (calcd. for $C_{20}H_{20}O_6Na$: 379.1158); ESI-MS^2 *m/z* (rel.int.) 357 $[M-H]^+$, 339 $[(M-H_2O)-H]^+$ (60), 311 $[(M-HCOOH)-H]^+$(20).

Compound **9**: Amorphous solid; $[\alpha]_D^{25}$ -67 (*c* 0.1, CH_3OH); UV/vis λ_{max} (CH_3OH) nm (log ε) 204 (3.98); ECD (CH_3OH, *c* 0.3 mM, 0.1 cm); $\Delta\varepsilon$ +2.2 (215 nm), -4.4 (243 nm); IR (KBr) ν_{max} (cm^{-1}) 3420, 2962, 2927, 2866, 1743, 1656, 1638, 1510, 1455, 1435, 1373, 1259, 1163, 1113, 1080, 1033, 872, 797, 603; ^{1}H NMR and ^{13}C NMR data, see Tables 1 and 2; HRESIMS (positive ion mode) *m/z* 615.2393 $[M+Na]^+$ (calcd. for $C_{30}H_{40}O_{12}Na$: 615.2417); ESI-MS^2 *m/z* (rel.int.) 615 $[M+Na]^+$, 555 $[M-CH_3COOH)+Na]^+$ (98), 461 $[(M-C_8H_{10}O_3)+Na]^+$ (3), 333 $[(M-C_8H_{14}O_7)+Na]$ (2).

Compound **12**: Amorphous solid; $[\alpha]_D^{25}$ -27 (*c* 0.5, CH_3OH); ECD (CH_3OH, *c* 0.4 mM, 0.1 cm); $\Delta\varepsilon$ -6.0 (198 nm), -0.6 (215 nm), -7.3 (242 nm); UV/vis λ_{max} (CH_3OH) nm (log ε) 208 (4.13); IR (KBr) ν_{max} (cm^{-1}) 3406, 3083, 2929, 1756, 1740, 1656, 1634, 1608, 1455, 1384, 1359, 1293, 1231, 1194, 1157,

1084, 1028, 962, 891, 874. 787, 742; ^{1}H NMR and ^{13}C NMR data, see Tables 2 and 3; HRESIMS (positive ion mode) *m/z* 397.2813 $[M+Na]^+$ (calcd. for $C_{20}H_{22}O_7$: 397.1263); ESI-MS^2 *m/z* (rel.int.) 397 $[M+Na]^+$, 379 $[(M-H_2O)+Na]^+$ (10), 335 $[(M-H_2O-CO_2)+Na]^+$ (4).

Derivatization of Compounds 1, 3 and 11. Solutions of 1 (2.0 mg), 3 (1.5 mg), and 12 (2.0 mg) in dry acetone (1 mL) were treated with an excess of 2,2-dimethoxypropane (100 μL) and a catalytic amount of p-toluenesulfonic acid following the procedure of Ihre et al.(44) to obtain the corresponding acetonides. 1H NMR spectra of the acetonide derivatives of 1 and 12 are shown in the Supporting Information (Figures S6 and S34).

Determination of the sugar unit in compound 9. The absolute configuration of the sugar unit in compound 9 was performed according to Tanaka et al.(37) Cysteine methyl ester hydrochloride was prepared from cysteine, which was first converted into the corresponding hydrochloride(45) and subsequently into the methyl ester following the procedure of Wang et al.(46) IR and NMR data were in agreement with literature values. The NMR spectra were acquired in D2O, as DMSO-d6 causes oxidation of the cysteine and its derivatives also under mild conditions.(47) A Symmetry 300 C18 column (4.6 × 250 mm i.d., 5 μm particle size, Waters) was used for analytical HPLC.

Computational Methods. Conformational analysis of 1, 3, 4, 7, 8, 9, and 12 was performed with Schrödinger MacroModel 9.8 (Schrödinger, LLC, New York, NY, USA) employing the OPLS2005 (optimized potential for liquid simulations) force field in H2O. Conformers within a 5 kcal/mol energy window from the global minimum were selected for geometrical optimization and energy calculation applying DFT with the Becke's nonlocal three-parameter exchange and correlation functional and the Lee–Yang–Parr correlation functional level (B3LYP), using the B3LYP/6-31G** basis set in the gas phase with the Gaussian 09 program package.(48) Vibrational evaluation was done at the same level to confirm minima. The excitation energy (denoted by wavelength in nm), rotatory strength dipole velocity (Rvel), and dipole length (Rlen) were calculated in CH3OH by TD-DFT/CAM-B3LYP/6-31G**, using the SCRF method, with the CPCM model. ECD curves were obtained on the basis of rotatory strengths with a half-band of 0.16 eV and UV shift using SpecDis v1.61.(49) ECD spectra were calculated from the spectra of individual conformers according to their contribution calculated by Boltzmann-weighting.

α-Glucosidase inhibition assay. α-Glucosidase inhibitory activity was evaluated as previously reported.(38) Briefly, to each well were added 10 mM phosphate buffer pH 7.0 (130 μL) and the substrate 2.5 mM 4-nitrophenyl α-d-glucopyranoside in 10 mM phosphate buffer (60 μL) to a sample

(40 μL) dissolved in DMSO at different concentrations. The reaction was initiated by the addition of α-glucosidase enzyme (20 μL at 0.28 unit/mL in 10 mM phosphate buffer). The plates were incubated at 37 °C for 10 min. The absorbance was measured at 405 nm before (T0′) and after the incubation with the enzyme (T10′). Acarbose was used as positive control, and negative control absorbance (phosphate buffer in place of sample) was also recorded. Inhibition of the enzyme was calculated, and the results were expressed as IC50 values.

α-Amylase inhibition assay. Inhibition of α-amylase was assayed using 20 mM sodium phosphate buffer with 6 mM NaCl (10 μL, pH 6.9) containing 0.5 mg/mL of α-amylase (50 units/mg). A test sample or acarbose (10 μL) in DMSO at different concentrations was added, and the resulting solutions were preincubated at 25 °C for 10 min. Then, a 1% starch solution in 20 mM sodium phosphate buffer (10 μL) was added to each sample, and the reaction mixtures were incubated at 25 °C for 10 min. Dinitrosalicylic acid color reagent (20 μL) was added, and the test tubes were incubated in a boiling water bath for 10 min and cooled to room temperature. Finally, distilled water (300 μL) was added, and the absorbance measured at 540 nm. The absorbance of blank samples (the enzyme solution was added during the boiling) and negative control (sodium phosphate buffer was used in place of sample) was recorded. Inhibition of the α-amylase activity was calculated, and results were expressed as IC50 values.

Statistical Analysis. All determinations were done in triplicate, and the results reported as mean ± standard deviation (SD). Calculation of IC50 values was done by nonlinear curve fitting, using GraphPad Prism version 5 for Windows (GraphPad Software Inc., San Diego, CA, USA). Data were considered statistically significant at $p \leq 0.05$.

Molecular Modeling. Compound 3 was built using the tools of Maestro software and was then energy minimized employing a water environment model (generalized-Born/surface-area model) by means of Macromodel. Minimization was performed employing the MMFF force field, the conjugated gradient method, and a distance-dependent dielectric constant of 1.0, until a convergence value of 0.05 kcal/(mol·Å2) was reached. Compound 3 was docked into the binding pocket of the recently published model of the α-1,4-glucosidase receptor by means of AUTODOCK4.2.(40) The docking site used for calculation was defined by superimposing the generated model to the template structure (PDB code 3A4A) and setting the crystallographic ligand (maltose) as the central group of a grid of 56 points respectively in the x, y, and z directions. Calculation of energetic maps was carried out by using a grid spacing of 0.375 Å and a distance-dependent function of the dielectric constant. Compound 3 was subjected to 200 runs of an AUTODOCK calculation using a robust procedure with 10 000 000 steps of

energy evaluation. The number of individuals in the initial population was set to 500, and a maximum of 10 000 000 generations was simulated in each docking run. An RMSD threshold of 2.0 Å was applied in order to cluster the docking solutions, and all the other settings were left as defaults. A single cluster containing all 200 poses generated was obtained; thus a representative docking pose was chosen and subjected to further studies. The MD simulation was performed by means of AMBER14.(50) The procedure applied was the same previously set up using as reference structure the X-ray complex of oligo-1,6-glucosidase with maltose.(39) The α-glucosidase–compound 3 complex obtained from the docking calculation was placed in a cubic water box and solvated with a 20 Å water cap. An explicit solvent model for water was used (TIP3P). The General Amber Force Field parameters were designed for compound 3, whereas the partial charges were calculated by means of the AM1-BCC as implemented in the Antechamber suite. Sodium ions were added as counterions in order to neutralize the system. Before running MD simulations, the ligand–protein complex was energy-minimized by means of 1000 steps of steepest descent followed by 2000 steps of conjugate gradient, for a total of 3000 steps of energy minimization, until a convergence of 0.05 kcal/(mol·Å2) was reached. A position restraint of 10.0 kcal/(mol·Å2) was applied to the protein α carbons in order to block the protein backbone. The minimized complex so obtained was employed as the starting conformation to run the MD trajectory; particle mesh Ewald electrostatics and periodic boundary conditions were used in the simulation.(51) Three different steps of MD simulations were run employing a cutoff of 10 Å for the nonbonded interactions and the SHAKE algorithm to keep rigid every bond involving hydrogen. A first MD step, consisting of 0.5 ns of constant-volume simulation, was conducted in order to increase the temperature from 0 K to 300 K. In the second step, 3.5 ns of constant-pressure simulation was carried out to equilibrate the system; thus, the temperature was maintained constant at 300 K using a Langevin thermostat. As in the previous minimization stage, in both these steps, a harmonic force of 10 kcal/(mol·Å2) was applied to clamp the protein α carbon. At the least, a third step of 36.5 ns was performed by using the same conditions employed in step two; no position constraints were applied to the complex in order to leave the whole system free to move. Therefore, a total of 50 ns of molecular dynamic simulation was performed for the α-glucosidase–compound 3 complex.

Antimicrobial Activity. Altogether, 26 clinical strains, previously isolated from different clinical specimens and identified according to standard procedures,(52) were used. All strains were deposited in the collection of the Microbiology Central Laboratory of the San Martino Hospital (Laboratorio di Analisi Chimico-Cliniche e Microbiologia, IRCCS Azienda Ospedaliera Universitaria San Martino IST, Istituto Nazionale per la Ricerca sul Cancro, Largo R. Benzi 10-16132 Genova, Italy) (code of

strains indicating the location of the collection: MB). Eighteen strains belonged to six Gram-positive species [Staphylococcus aureus, S. epidermidis, Streptococcus agalactiae, S. pneumoniae (MB 35), Enterococcus faecium, and E. faecalis], four were clinical strains of Gram-negative species [Escherichia coli (MB 123), Proteus mirabilis (MB 14), Moraxella catarrhalis (MB 15), and Klebsiella pneumoniae (MB 11)], and two were clinical strains of fungi [Candida albicans (MB 31) and C. glabrata (MB 8)]. Among the Gram-positive organisms, one S. aureus strain was methicillin-susceptible (MSSA) (MB 21) and three were methicillin- and multidrug-resistant (MRSA)(53, 54) (MB 9, MB 10, MB 18). One S. epidermidis was methicillin-susceptible (MSSE) (MB 65), and three were methicillin- and multidrug-resistant (MRSE) (MB 20, MB 26, MB 64). One E. faecalis was vancomycin-susceptible (MB 3), and three were vancomycin-resistant (VRE) (MB 1, MB 49, MB 51). One E. faecium was vancomycin-susceptible (MB 55), and three were VRE (MB 2, MB 23, MB 50). One strain of antibiotic-susceptible S. agalactiae (MB 27) and S. pyogenes (MB 9) were also included. The preparation of solutions of test compounds and control antibiotics as well as susceptibility testing was performed as previously described.(9) MICs were determined following the microdilution procedure as detailed.(9)

Supporting Information. NMR spectra of compounds 1, 3, 4, 7, 8, 9, and 12; dose-dependent α-glucosidase and α-amylase inhibition of acarbose and active fractions; and MD simulations analysis.

Notes

The authors declare no competing financial interest.

Ackowledgements. ECD spectra were measured at the Biophysics Facility, Biozentrum, University of Basel.

References

ARTICLE SECTIONSJump To

This article references 54 other publications.

1 Bisio, A.; Damonte, G.; Fraternale, D.; Giacomelli, E.; Salis, A.; Romussi, G.; Cafaggi, S.; Ricci, D.; De Tommasi, N. Phytochemistry 2011, 72, 265– 275 DOI: 10.1016/j.phytochem.2010.11.011

2 Bisio, A.; Fraternale, D.; Giacomini, M.; Giacomelli, E.; Pivetti, S.; Russo, E.; Caviglioli, G.; Romussi, G.; Ricci, D.; De Tommasi, N. Crop Prot. 2009, 29, 1434– 1446 DOI: 10.1016/j.cropro.2010.08.002

3 Bisio, A.; Schito, A. M.; Parricchi, A.; Mele, G.; Romussi, G.; Malafronte, N.; Oliva, P.; De Tommasi, N. Phytochem. Lett. 2015, 14, 170– 177 DOI: 10.1016/j.phytol.2015.10.005

4 Epling, C. A Revision of Salvia, Subgenus Calosphace; University of California Press: Berkeley, CA, 1939, 1940; Vol. 110, p 383.

5 Fernald, M. L. A Synopsis of the Mexican and Central American Species of Salvia; Proceedings of the American Academy: Cambridge, MA, 1900; Vol. 35, pp 489– 556.

6 Turner, B. L. Phytoneuron 2013, 36, 1– 11

7 Jenks, A. A.; Walker, J. B.; Kim, S. C. J. Plant Res. 2013, 126, 483– 496 DOI: 10.1007/s10265-012-0543-1

8Bisio, A.; De Tommasi, N.; Romussi, G. Planta Med. 2004, 70, 452– 457 DOI: 10.1055/s-2004-818975

9 Bisio, A.; Schito, A. M.; Ebrahimi, S. N.; Hamburger, M.; Mele, G.; Piatti, G.; Romussi, G.; Dal Piaz, F.; De Tommasi, N. Phytochemistry 2015, 110, 120– 132 DOI: 10.1016/j.phytochem.2014.10.033

10 Bisio, A.; Fontana, N.; Romussi, G.; Ciarallo, G.; De Tommasi, N.; Pizza, C.; Mugnoli, A. Phytochemistry 1999, 52, 1535– 1540 DOI: 10.1016/S0031-9422(99)00324-6

11 Bisio, A.; Romussi, G.; Russo, E.; Cafaggi, S.; Fraternale, D.; De Tommasi, N. Planta Med. 2008, 74, 1041– 1041

12 Rodriguez-Hahn, L.; Esquivel, B.; Càrdenas, J. In Progress in the Chemistry of Organic Natural Products; Herz, W.; Kirby, G. W.; Moore, R. E.; Steglich, W.; Tamm, C., Eds.; Springer-Verlag: Vienna, 1994; Vol. 63, pp 107– 196.

13 Calzada, F.; Bautista, E.; Yépez-Mulia, L.; García-Hernandez, N.; Ortega, A. Phytother. Res. 2015, 29, 1600– 1604 DOI: 10.1002/ptr.5421

14 Wu, Y. B.; Ni, Z. Y.; Shi, Q. W.; Dong, M.; Kiyota, H.; Gu, Y. C.; Cong, B. Chem. Rev. 2012, 112, 5967– 6026 DOI: 10.1021/cr200058f

15 Yu, B. C.; Hung, C. R.; Chen, W. C.; Cheng, J. T. Planta Med. 2003, 69, 1075– 1079 DOI: 10.1055/s-2003-45185

16 Bnouham, M.; Ziyyat, A.; Mekhfi, H.; Tahri, A.; Legssyer, A. Int. J. Diabetes Metabol. 2006, 14, 1– 25

17 de Sales, P. M.; Monteiro de Souza, P.; Simeoni, L. A.; de Oliveira Magalhães, P.; Silveira, D. J. Pharm. Pharm. Sci. 2012, 15, 141– 183 DOI: 10.18433/J35S3K

18 Mahmood, N. Comp. Clin. Pathol. 2016, 25, 1253– 1264 DOI: 10.1007/s00580-014-1967-x

19 Kumar, S.; Narwal, S.; Kumar, V.; Prakash, O. Pharmacogn. Rev. 2011, 5, 19– 29 DOI: 10.4103/0973-7847.79096

20 Tundis, R.; Loizzo, M. R.; Menichini, F. Mini-Rev. Med. Chem. 2010, 10, 315– 331 DOI: 10.2174/138955710791331007

21 Abreu, A. C.; Borges, A.; Malheiro, J.; Simões, M. In Microbial Pathogens and Strategies for Combating Them: Science, Technology and Education; Méndez-Vilas, A., Ed.; Formatex Research Center: Badajoz, Spain, 2013; Vol. 2, pp 1287– 1297.

22 Bisio, A.; Fraternale, D.; Schito, A. M.; Parricchi, A.; Dal Piaz, F.; Ricci, D.; Giacomini, M.; Ruffoni, B.; De Tommasi, N. Phytochemistry 2016, 122, 276– 285 DOI: 10.1016/j.phytochem.2015.12.017

23 Bisio, A.; Romussi, G.; Russo, E.; Cafaggi, S.; Schito, A. M.; Repetto, B.; De Tommasi, N. J. Agric. Food Chem. 2008, 56, 10468– 10472 DOI: 10.1021/jf802200x

24 Bautista, E.; Toscano, R. A.; Ortega, A. J. Nat. Prod. 2014, 77, 1088– 1092 DOI: 10.1021/np4009893

25 Gigovich, A.; San-Martin, A.; Castillo, M. Phytochemistry 1986, 25, 2829– 2831 DOI: 10.1016/S0031-9422(00)83751-6

26 Rodriguez-Hahn, L.; O'Reilly, R.; Esquivel, B.; Maldonado, E.; Ortega, A.; Cárdenas, J.; Toscano, R. A. J. Org. Chem. 1990, 55, 3522– 3525 DOI: 10.1021/jo00298a026

27 Pan, Z. H.; Cheng, J. T.; He, J.; Wang, Y. Y.; Peng, L. Y.; Xu, G.; Sun, W. B.; Zhao, Q. S. Helv. Chim. Acta 2011, 94, 417– 421 DOI: 10.1002/hlca.201000203

28 Dhooghe, L.; Mesia, K.; Kohtala, E.; Tona, L.; Pieters, L.; Vlietinck, A. J.; Apers, S. Talanta 2008, 76, 462– 468 DOI: 10.1016/j.talanta.2008.03.036

29 Nakatani, N.; Inatani, R. Agric. Biol. Chem. 1981, 45, 2385– 2386 DOI: 10.1271/bbb1961.45.2385

30 Inatani, R.; Nakatani, N.; Fuwa, H.; Seto, H. Agric. Biol. Chem. 1982, 46, 1661– 1666 DOI: 10.1271/bbb1961.46.1661

31 Merrit, A. T.; Ley, S. V. Nat. Prod. Rep. 1992, 9, 243– 287 DOI: 10.1039/np9920900243

32 Ali, M. E.; Owen, L. N. J. Chem. Soc. 1958, 2119– 2129 DOI: 10.1039/jr9580002119

33 Manabe, S.; Nishino, C. Tetrahedron 1986, 42, 3461– 3470 DOI: 10.1016/S0040-4020(01)87313-0

34 Fontana, G.; Savona, G.; Rodriguez, B. J. Nat. Prod. 2006, 69, 1734– 1738 DOI: 10.1021/np068036d

35 Bohlmann, F.; Zdero, C.; Hunecka, S. Phytochemistry 1985, 24, 1027– 1030 DOI: 10.1016/S0031-9422(00)83175-1

36 Li, M. M.; Wang, K.; He, J.; Peng, L. Y.; Chen, X. Q.; Cheng, X.; Zhao, Q. S. Nat. Prod. Bioprospect. 2013, 3, 38– 42 DOI: 10.1007/s13659-012-0022-3

37 Tanaka, T.; Nakashima, T.; Ueda, T.; Tomii, K.; Kouno, I. Chem. Pharm. Bull. 2007, 55, 899– 901 DOI: 10.1248/cpb.55.899

38 Saltos, M. B. V.; Puente, B. F. N.; Faraone, I.; Milella, L.; De Tommasi, N.; Braca, A. Phytochem. Lett. 2015, 14, 45– 50 DOI: 10.1016/j.phytol.2015.08.018

39 Milella, L.; Milazzo, S.; De Leo, M.; Vera Saltos, M. B.; Faraone, I.; Tuccinardi, T.; Lapillo, M.; De Tommasi, N.; Braca, A. J. Nat. Prod. 2016, 79, 2104– 2112 DOI: 10.1021/acs.jnatprod.6b00484

40 Morris, G. M.; Huey, R.; Lindstrom, W.; Sanner, M. F.; Belew, R. K.; Goodsell, D. S.; Olson, A. J. J. Comput. Chem. 2009, 30, 2785– 2791 DOI: 10.1002/jcc.21256

41 Yamamoto, K.; Miyake, H.; Kusunoki, M.; Osaki, S. FEBS J. 2010, 277, 4205– 4214 DOI: 10.1111/j.1742-4658.2010.07810.x

42 Asghari, B.; Salehi, P.; Sonboli, A.; Nejad Ebrahimi, S. Iran. J. Pharm. Res. 2015, 14, 609– 615

43 Nickavar, B.; Abolhasani, L.; Izadpanah, H. Iran. J. Pharm. Res. 2008, 7, 297– 303

44 Ihre, H.; Hult, A.; Frechet, J. M. J.; Gitsov, I. Macromolecules 1998, 31, 4061– 4068 DOI: 10.1021/ma9718762

45 Liwschitz, Y.; Zilkha, A.; Shahak, I. J. Org. Chem. 1956, 21, 1530 DOI: 10.1021/jo01118a614

46 Wang, P.; Liu, H.; Zhao, Q.; Chen, Y.; Liu, B.; Zhang, B.; Zheng, Q. Eur. J. Med. Chem. 2014, 74, 199– 215 DOI: 10.1016/j.ejmech.2013.12.041

47 Papanyan, Z.; Markarian, S. J. Appl. Spectrosc. 2013, 80, 775– 778 DOI: 10.1007/s10812-013-9841-1

48 Frisch, M. J.; Trucks, G. W.; Schlegel, H. B.; Scuseria, G. E.; Robb, M. A.; Cheeseman, J. R.; Scalmani, G.; Barone, V.; Mennucci, B.; Petersson, G. A.; Nakatsuji, H.; Caricato, M.; Li, X.; Hratchian, H. P.; Izmaylov, A. F.; Bloino, J.; Zheng, G.; Sonnenberg, J. L.; Hada, M.; Ehara, M.; Toyota, K.; Fukuda, R.; Hasegawa, J.; Ishida, M.; Nakajima, T.; Honda, Y.; Kitao, O.; Nakai, H.; Vreven, T.; Montgomery, J. A.; Peralta, J. E.; Ogliaro, F.; Bearpark, M.; Heyd, J. J.; Brothers, E.;

Kudin, K. N.; Staroverov, V. N.; Kobayashi, R.; Normand, J.; Raghavachari, K.; Rendell, A.; Burant, J. C.; Iyengar, S. S.; Tomasi, J.; Cossi, M.; Rega, N.; Millam, J. M.; Klene, M.; Knox, J. E.; Cross, J. B.; Bakken, V.; Adamo, C.; Jaramillo, J.; Gomperts, R.; Stratmann, R. E.; Yazyev, O.; Austin, A. J.; Cammi, R.; Pomelli, C.; Ochterski, J. W.; Martin, R. L.; Morokuma, K.; Zakrzewski, V. G.; Voth, G. A.; Salvador, P.; Dannenberg, J. J.; Dapprich, S.; Daniels, A. D.; Farkas, O.; Foresman, J. B.; Ortiz, J. V.; Cioslowski, J.; Fox, D. J.Gaussian 09, Revision A02; Gaussian, Inc.: Wallingford, CT, 2009.

49 Bruhn, T.; Schaumlöffel, A.; Hemberger, Y.; Bringmann, G.SpecDis version 1.61; University of Wuerzburg: Wuerzburg, Germany, 2013.

50 Case, D. A.; Berryman, J. T.; Betz, R. M.; Cerutti, D. S., III; C, T. E.; Darden, T. A.; Duke, R. E.; Giese, T. J.; Gohlke, H.; Goetz, A. W.; Homeyer, N.; Izadi, S.; Janowski, P.; Kaus, J.; Kovalenko, A.; Lee, T. S.; LeGrand, S.; Li, P.; Luchko, T.; Luo, R.; Madej, B.; Merz, K. M.; Monard, G.; Needham, P.; Nguyen, H.; Nguyen, H. T.; Omelyan, I.; Onufriev, A.; Roe, D. R.; Roitberg, A.; Salomon-Ferrer, R.; Simmerling, C. L.; Smith, W.; Swails, J.; Walker, R. C.; Wang, J.; Wolf, R. M.; Wu, X.; York, D. M.; Kollman, P. A.AMBER, version 14; University of California: San Francisco, CA, 2015.

51 York, D. M.; Darden, T. A.; Pedersen, L. G. J. Chem. Phys. 1993, 99, 8345– 8348 DOI: 10.1063/1.465608

52 Murray, P. R.; Baron, E. J.; Pfaller, M. A.; Tenover, F. C.; Yolken, R. H. Manual of Clinical Microbiology, 7th ed.; American Society for Microbiology Press: Washington, DC, 1999.

53 Clinical and Laboratory Standards Institute. Reference Method for Broth Dilution Antifungal Susceptibility Testing of Yeasts; Approved Standard, Third Edition. CLSI Document M27-A3; Clinical and Laboratory Standards Institute: Wayne, PA, 2008.

54 Clinical and Laboratory Standards Institute. Performance Standards for Antimicrobial Susceptibility Testing; 16th Informational Supplement; CLSI M100-S20; Clinical and Laboratory Standards Institute: Wayne, PA, 2010.

Table 1. 1H and 13C NMR data of Compounds **1**, **3** and **7** ($CDCl_3$, 600 MHz)[a]

	1			**3**			**7**		
position	δ_C, type		HMBC[b]	δ_C, type		HMBC[b]	δ_C, type		HMBC[b]
1	20.5 , CH_2	1.26 dddd (12.7, 12.6, 12.6, 3.8) (α) 1.70 m (β)	2, 3, 5, 9, 10	75.7 , CH	4.54 ddd (8.0, 3.2, 1.3) (α)	3, 5, 9	132.1 , CH	5.90 dd (9.9, 2.3)	3, 5
2	27.2 , CH_2	2.47 dddd (18.0, 7.1, 3.8, 1.7) (α) 2.25[b] (β)	1, 3, 4, 10, 18	31.3 , CH_2	3.07 ddd (20.2, 8.0, 6.2) (α) 2.70 ddd (20.2, 1.6, 1.3) (β)	1, 3, 4, 10	123.0 , CH	6.22 dd (9.9, 5.3)	-
3	134.3 , CH	6.74 dd (7.4, 1.7)	1, 2, 5, 18	134.0 , CH	6.88 dd (6.2, 1.6)	1, 2, 5, 18	129.0 , CH	6.87 d (5.3)	1, 2, 5, 18
4	138.2 , C	-	-	137.8 , C	-	-	128.5 , C	-	-
5	44.1 , C	-	-	40.6 , C	-	-	39.5 , C	-	-
6	38.3 , CH_2	2.04[b] 2.08[b]	4, 5, 7, 8, 10, 19	39.7 , CH_2	2.02[b] 2.20 m	4, 5, 7, 8, 10	32.5 , CH_2	1.91 dd (14.6, 8.5) (α) 2.20 dd (14.6, 9.5) (β)	4, 5, 7, 8, 10, 19
7	69.2 , CH	4.49 t (6.7, 6.7)	5, 6, 17	69.5 , CH	4.41 dd (8.0, 1.0)	5, 6, 8, 9, 17	63.3 , CH	4.69 ddd (9.0, 8.0, 3.9)	6, 8
8	78.0 , C	-	-	81.6 , C	-	-	47.3 , CH	2.32 d (3.9)	7, 9, 10, 11, 17, 20
9	40.7 , C	-	-	40.0 , C	-	-	34.6 , C	-	-
10	43.5 , CH	2.01[b]	1, 2, 5, 6, 8, 11, 19, 20	58.0 , CH	1.96 d (3.2)	5, 6, 8, 9, 11, 19	53.2 , CH	2.92 d (2.3)	1, 5, 6, 9, 19
11	41.0 , CH_2	1.98[b] 2.15[b]	8, 9, 10, 12, 13, 20	45.0 , CH_2	2.01[b] 2.08[b]	8, 9, 10, 12, 13, 20	49.5 , CH_2	2.07 dd (15.4, 12.3) (α) 2.27 dd (15.4, 3.0) (β)	8, 9, 10, 12, 13, 20
12	71.3 , CH	5.53 dd (12.3, 2.4)	9, 11, 13, 14, 16	72.6 , CH	5.76 dd (12.0, 3.7)	11, 13, 14, 16	71.5 , CH	5.33 dd (12.3, 3.0)	13, 14, 16
13	124.2 , C	-	-	124.1 , C	-	-	123.2 , C	-	-
14	108.4 , CH	6.46 br s	12, 13, 15, 16	108.6 , CH	6.45 br s	13, 15, 16	108.8 , CH	6.44 br s	13, 15, 16
15	144.4 , CH	7.45 br s	13, 16	144.3 , CH	7.45 br s	13, 16	144.4 , CH	7.45 br s	13, 14, 16
16	140.3 , CH	7.52 br s	13, 14, 15	140.3 , CH	7.50 br s	13, 14, 15	140.4 , CH	7.50 br s	14, 15
17	174.2 , C	-	-	171.3 , C	-	-	173.8 , C	-	-
18	169.1 , C	-	-	168.5 , C	-	-	169.1 , C	-	-
19	74.3 , CH_2	4.01 dd (7.6; 1.8) (*pro S*) 5.04 d (7.6) (*pro R*)	4, 5, 6, 10, 18	80.8 , CH_2	4.29 dd (9.2, 1.0) (*pro S*) 4.70 d (9.2) (*pro R*)	4, 5, 6, 10, 18	79.2 , CH_2	3.96 dd (7.9, 2.1) (*pro S*) 4.36 d (7.9) (*pro R*)	4, 5, 6, 10, 18
20	20.2 , CH_3	0.98 s	8, 9, 10, 11, 12	23.6 , CH_3	1.49 s	8, 9, 10, 11	28.6 , CH_3	1.37 s	8, 9, 10, 11

[a] *J* values are in parentheses and reported in Hz; chemical shifts are given in ppm; assignments were confirmed by DQF-COSY, 1D-TOCSY and HSQC experiments. [b] Overlapped signal.

Table 2. 1H and 13C NMR data of Compounds **4** and **9** ($CDCl_3$, 600 MHz)[a]

	4					**9**				
position	δ_C, type				HMBC[b]	δ_C, type				HMBC[b]
1	124.4	,	CH	6.07 dd (16.3, 3.4)	2, 3, 9, 10	20.0	,	CH_2	1.12 m	2, 3, 5, 9, 10
									1.50 m	
2	133.8	,	CH	6.35 dd (11.7, 3.4)	3, 4	27.6	,	CH_2	2.06 m	1, 3, 4, 10
									2.31 m	
3	122	,	CH	6.15 d (11.7)	4	135.9	,	CH	6.70 dd (8.8, 2.2)	1, 2, 5, 18
4	152.9	,	C	-	-	139.0	,	C	-	-
5	125.2	,	C	-	-	45.3	,	C	-	-
6	35.4	,	CH_2	3.73 dd (14.1, 13.2) (α)	4, 5, 7, 8	36.4	,	CH_2	1.27 dd (14.4, 1.1)	5, 7, 8, 10, 19
				2.60 dd (14.1, 5.3) (β)					2.40 dd (14.4, 1.2)	
7	71	,	CH	4.64 ddd (13.2, 5.3, 2.0)	5, 6, 8, 9	79.1	,	CH	4.03 ddd (2.0, 1.2, 1.1)	-
8	48	,	CH	2.50 d (2.0)	17	41.5	,	CH	1.76[b]	9, 10, 11, 17, 20
9	39.3	,	C	-	-	39.3	,	C	-	-
10	141	,	CH	6.00 d (16.3)	1, 2, 8, 9, 11, 20	48.7	,	CH	1.88 dd (12.3, 1.0)	1, 2, 5, 6, 8, 9, 19, 20
11	45.7	,	CH_2	2.13 dd (14.8, 3.0) (α)	9, 10, 12, 13, 20	43.3	,	CH_2	2.23 dd (16.1, 7.5)	8, 9, 10, 12, 13, 20
				1.94 dd (14.8, 12.3) (β)					1.78[b]	
12	71.4	,	CH	5.33 dd (12.3, 3.0)	13, 16	64.9	,	CH	5.82 dd (7.5, 2.0)	9, 11, 13, 14, 16, 1"
13	123.2	,	C	-	-	126.5	,	C	-	-
14	108.7	,	CH	6.40 br s	13, 15, 16	108.9	,	CH	6.41 br s	13, 15, 16
15	144.4	,	CH	7.42 br s	13, 16	143.8	,	CH	7.39 br s	13, 16
16	140.3	,	CH	7.47 br s	14, 15	140.3	,	CH	7.42 br s	14, 15
17	175.3	,	C	-	-	12.5	,	CH_3	1.12 d (6.7)	7, 8, 9
18	174.8	,	C	-	-	170.0	,	C	-	-
19	72	,	CH_2	4.70[b]	4, 5, 18	72.7	,	CH_2	3.84 dd (7.7, 1.1) (*pro S*)	4, 5, 6, 18
				4.71[b]					5.30 d (7.7) (*pro R*)	
20	24.5	,	CH_3	1.57 s	8, 9, 10, 11	19.9	,	CH_3	0.80 s	8, 9, 10, 11
1'	-			-	-	101.1	,	CH	4.32[b]	7, 2'
2'	-			-	-	74.2	,	CH	3.37[b]	1', 3'
3'	-			-	-	77.1	,	CH	3.38[b]	1', 2'
4'	-			-	-	70.5	,	CH	3.40[b]	3', 5', 6'
5'	-			-	-	77.4	,	CH	3.54 ddd (9.8, 8.0, 1.8)	3', 4'
6'	-			-	-	63.5	,	CH_2	4.30[b]	4', 5', 1"
				-					4.48 dd (12.3, 1.8)	
1"	-			-	-	172.3	,	C	-	-
2"	-			-	-	21.2	,	CH_3	2.12 s	6', 1"
1"'	-			-	-	170.6	,	C	-	-
2"'	-			-	-	21.6	,	CH_3	2.01 s	1"'

[a] *J* values are in parentheses and reported in Hz; chemical shifts are given in ppm; assignments were confirmed by DQF-COSY, 1D-TOCSY and HSQC experiments. [b] Overlapped signal.

Table 3. 1H and 13C NMR data of Compounds **8** and **12** ($CDCl_3$, 600 MHz)[a]

	8					**12**				
position	δ_C, type				HMBC[b]	δ_C, type				HMBC[b]
1	132.1	,	CH	6.07 dd (9.5, 2.1)	2,, 3, 4, 5, 9, 10	19.2	,	CH_2	1.28 dddd (12.8, 12.4, 12.4, 4.9) (α) 1.63 m (β)	2, 3, 5, 9, 10
2	127.3	,	CH	6.45 m	1, 3, 4, 10	27.8	,	CH_2	2.43 dddd (18.0, 7.5, 4.9, 1.8) (α) 2.27 dddd (18.0, 12.4, 6.8, 2.4) (β)	1, 3, 4, 10
3	128.2	,	CH	6.98 d (4.7)	1, 2, 5, 10, 18	135.7	,	CH	6.73 dd (6.8, 1.8)	1, 2, 5, 18
4	132.3	,	C	-	-	138.4	,	C	-	-
5	38.9	,	C	-	-	44.4	,	C	-	-
6	31.9	,	CH_2	1.97 m (α)	5, 7, 8, 10, 19	34.1	,	CH_2	1.83[b]	4, 5, 7, 8, 10, 19
				1.68 dd (14.2, 4.5) (β)					2.31[b]	
7	64.7	,	CH	4.52 m	6	72.3	,	CH	4.34 ddd (4.5, 2.2, 1.8)	5, 6, 8, 9
8	45.5	,	CH	2.69 d (2.6)	7, 9, 10, 11, 17, 20	75.5	,	C	-	-
9	35.4	,	C	-	-	39.4	,	C	-	-
10	50.6	,	CH	2.66 d (2.1)	1, 4, 5, 6, 8, 9, 11, 20	45.2	,	CH	2.52 dd (12.8, 1.8)	1, 2, 4, 5, 6, 8, 9, 11, 19
11	42.0	,	CH_2	1.89 dd (15.2, 12.5) (α)	8, 9, 10, 12, 13, 20	41.3	,	CH_2	1.81[b]	8, 9, 10, 12, 20
				2.54 dd (15.2, 4.3) (β)					2.34[b]	
12	72.0	,	CH	5.37 dd (12.5, 4.3)	11, 13, 14, 16	72.2	,	CH	5.98 dd (8.5, 1.2)	11, 13, 14, 16
13	123.2	,	C	-	-	126.0	,	C	-	-
14	108.6	,	CH	6.47 br s	13, 15, 16	108.6	,	CH	6.41 br s	13, 15, 16
15	144.2	,	CH	7.46 br s	13, 14, 16	144.2	,	CH	7.45 br s	13, 16
16	140.1	,	CH	7.52 br s	13, 14, 15	139.7	,	CH	7.46 br s	14, 15
17	174.3	,	C	-	-	172.7	,	C	-	-
18	169.9	,	C	-	-	169.7	,	C	-	-
19	78.4	,	CH_2	4.11 dd (8.6, 2.1) (*pro S*)	4, 5, 6, 10, 18	72.7	,	CH_2	3.93 dd (7.6, 2.2) (*pro S*)	4, 5, 6, 10, 18
				5.19 d (8.6) (*pro R*)					5.24 d (7.6) (*pro R*)	
20	29.6	,	CH_3	1.39 s	8, 9, 10, 11	20.1	,	CH_3	1.20 s	8, 9, 10, 11

[a] *J* values are in parentheses and reported in Hz; chemical shifts are given in ppm; assignments were confirmed by DQF-COSY, 1D-TOCSY and HSQC experiments. [b] Overlapped signal.

Table 4.

Bacterial strains	SE	III	IV	V	VI	VII	PG			O			A			V		
S.aureus																		
MB 9 (MRSA)	-	32	16	32	128	32	128	(	343.6	)	256	(604.6)		n.t.			n.t.	
MB 10 (MRSA)	-	16	8	16	128	64	128	(	343.6	)	256	(604.6)		n.t.			n.t.	
MB 18 (MRSA)	-	8	32	32	128	128	128	(	343.6	)	256	(604.6)		n.t.			n.t.	
MB 21 (MSSA)	-	32	16	32	128	64	128	(	343.6	)	0.25	(0.6)		n.t.			n.t.	
S.epidermidis																		
MB 20 (MRSE)	-	32	16	64	128	128	8	(	21.5	)	256	(604.6)		n.t.			n.t.	
MB 26 (MRSE)	-	64	32	64	128	64	8	(	21.5	)	256	(604.6)		n.t.			n.t.	
MB 64 (MRSE)	-	32	8	128	128	32	8	(	21.5	)	256	(604.6)		n.t.			n.t.	
MB 65 (MSSE)	-	64	16	64	128	64	32	(	85.9	)	0.25	(0.6)		n.t.			n.t.	
E. faecalis																		
MB 1 (VRE)	4	8	8	8	8	4	n.t.			n.t.			8	(21.5)		32	(21.5)	
MB 3	4	4	4	4	16	8	n.t.			n.t.			32	(86.2)		32	(21.5)	
MB 49 (VRE)	2	8	2	4	8	16	n.t.			n.t.			32	(86.2)		32	(21.5)	
MB 51 (VRE)	8	4	4	2	16	8	n.t.			n.t.			1	(2.7)		2	(1.3)	
E.faecium																		
MB 2 (VRE)	2	4	2	4	8	4	n.t.			n.t.			32	(86.2)		256	(172.3)	
MB 23 (VRE)	4	4	4	2	16	8	n.t.			n.t.			32	(86.2)		256	(172.3)	
MB 50 (VRE)	2	4	2	2	8	2	n.t.			n.t.			32	(86.2)		256	(172.3)	
MB 55	2	4	2	4	8	8	n.t.			n.t.			32	(86.2)		1	(0.7)	

MIC values, expressed in μg/mL and micromolarity (μM), of the surface extract (**SE**), of crude fractions (**III-VII**), compared to standard reference antibiotics. Fractions I and II are not reported, since the obtained MIC values for all the tested strains were >128 μg/ml. Only the susceptible species are shown here. MRSA: Methicillin resistant *S. aureus*; MRSE: Methicillin resistant *S. epidermidis*; VRE:

Vancomycin resistant Enterococcus; PG: Penicillin G potassium salt; O: Oxacillin sodium salt; A: Ampicillin sodium salt; V: Vancomycin hydrochloride; -: MIC values > 128 μg/mL; n.t.: not tested.

Table 5.

Bacterial strains	1	4	6	7	10	11	12
S.aureus							
MB 9 (MRSA)	-	-	-	-	-	-	-
MB 10 (MRSA)	-	-	-	-	-	-	-
MB 18 (MRSA)	-	-	-	-	-	-	-
MB 21 (MSSA)	-	-	-	-	-	-	-
S.epidermidis							
MB 20 (MRSE)	-	-	-	-	-	-	-
MB 26 (MRSE)	-	-	-	-	-	-	-
MB 64 (MRSE)	-	-	-	-	-	-	-
MB 65 (MSSE)	-	-	-	-	-	-	-
E. faecalis							
MB 1 (VRE)	-	64 (179.7)	-	-	128 (233.5)	64 (186.0)	64 (171.1)
MB 3	-	32 (89.9)	-	-	64 (116.7)	32 (93.0)	128 (342.1)
MB 49 (VRE)	-	64 (179.7)	-	-	128 (233.5)	64 (186.0)	64 (171.1)
MB 51 (VRE)	-	32 (89.9)	-	-	64 (116.7)	32 (93.0)	32 (85.5)
E.faecium							
MB 2 (VRE)	128 (342.1)	32 (89.9)	128 (380.8)	128 (359.4)	128 (233.5)	64 (186.0)	64 (171.1)
MB 23 (VRE)	128 (342.1)	64 (179.7)	128 (380.8)	-	-	32 (93.0)	128 (342.1)
MB 50 (VRE)	-	64 (179.7)	128 (380.8)	128 (359.4)	128 (233.5)	32 (93.0)	64 (171.1)
MB 55	128 (342.1)	32 (89.9)	128 (380.8)	-	-	64 (186.0)	128 (342.1)

MIC values, expressed in μg/mL and micromolarity (μM), of the pure compounds **1**, **4**, **6**, **7**, **10**, **11** and **12** on the selected bacterial strains. Fractions I and II are not reported, since the obtained MIC values for all the tested strains were >128 μg/ml. Only the susceptible species are shown here. MRSA: Methicillin resistant *S. aureus*; MRSE: Methicillin resistant *S. epidermidis*; VRE: Vancomycin resistant Enterococcus; -: MIC values > 128 μg/mL; n.t.: not tested.

Table 6. Inhibitory activity (IC_{50} in µg/mL) of fractions of *S. chamaedryoides* and acarbose against the enzymes α- amylase and α-glucosidase.

	α-Amylase inhibition IC_{50} µg/mL	**α-Glucosidase inhibition IC_{50} µg/mL**
Acarbose	66.5±2.5	484±30
FI	ND	ND
FII	ND	ND
FIII	ND	56.3±4.9
FIV	385±25	43.8±3.1
FV	255±19	25.9±1.5
FVI	434±30	32.4±2.9
FVII	ND*	32.2±3.1

ND (Not Determined) represents fractions with no inhibition activity at the tested concentrations. ND* (Not Determined) represents the fraction with 9,46±1,01% of inhibition at the highest initial concentration (5 mg/mL). The values are expressed as means ± SD.

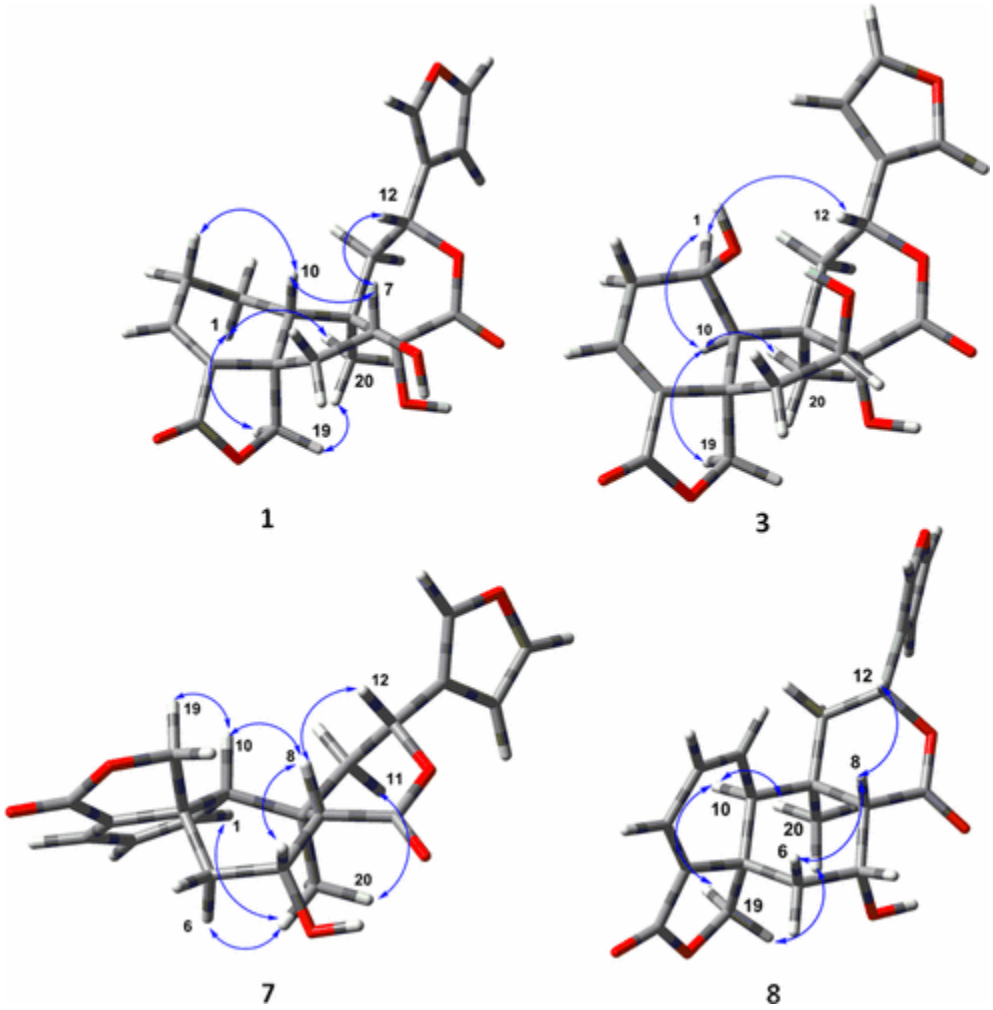

Figure 1. Geometrically optimized structures of compounds 1, 3, 7, and 8, with key ROESY correlations (blue arrows).

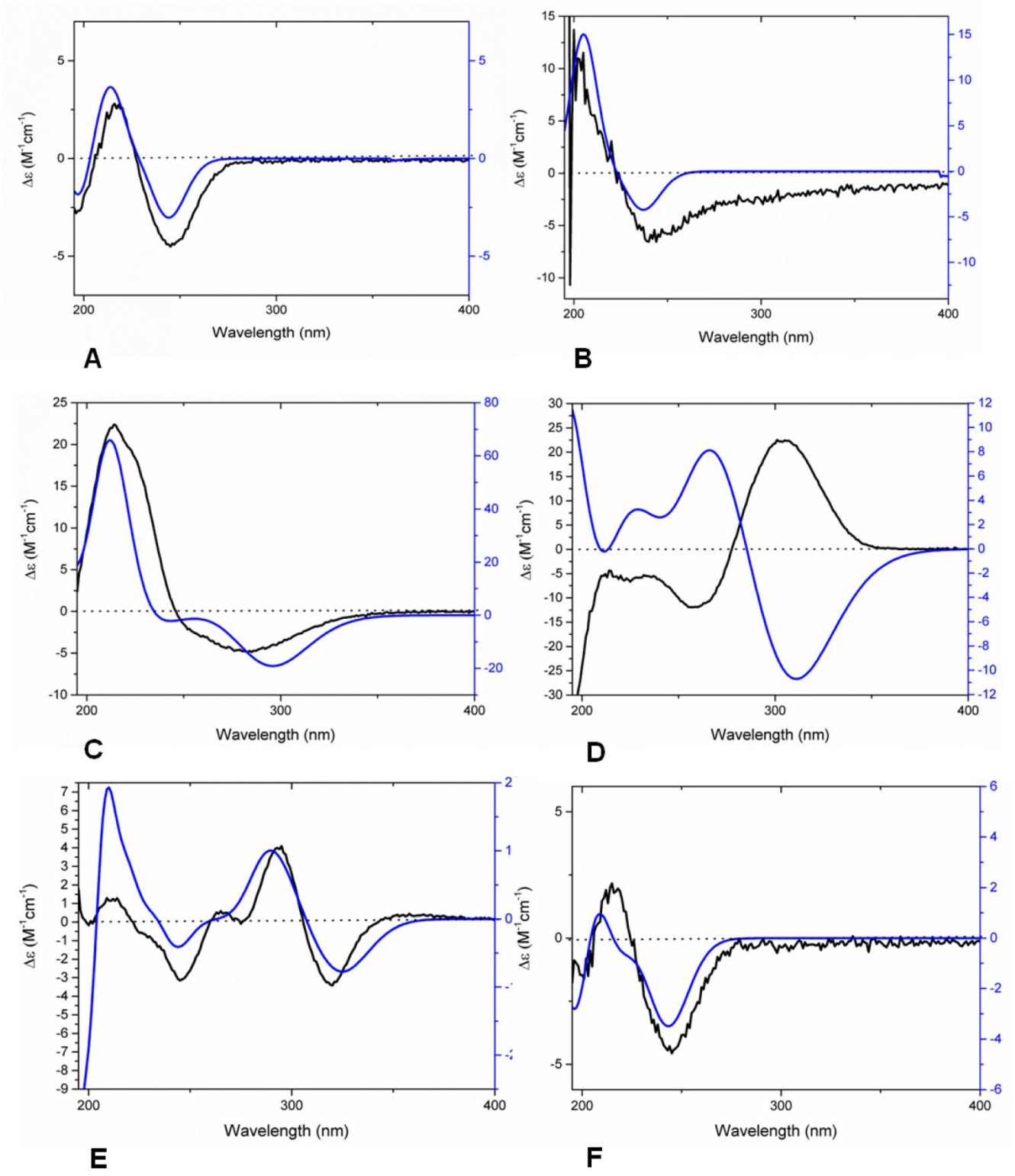

Figure 2. Experimental (black) and calculated (blue) ECD spectra of diterpenoids. (A) Compound 1. (B) Compound 3. (C) Compound 4. (D) Compound 7 (calculated for the ent-(5S,7S,8R,9S,10S,12S)-stereoisomer). (E) Compound 8. (F) Compound 9.

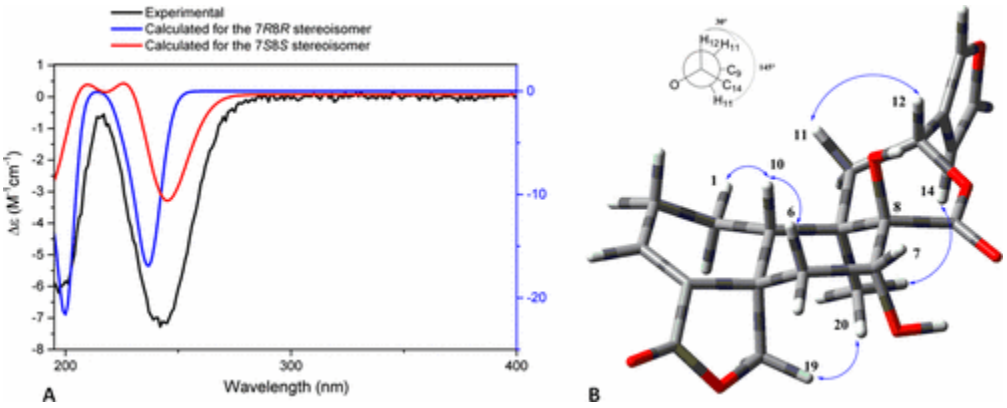

Figure 3. (A) Experimental ECD spectrum of compound **12** and calculated spectra for the 7*R*,8*R* and 7*S*,8*S* stereoisomers in CH_3OH. (B) Geometrically optimized structure of **12** with key ROESY correlations (blue arrows). The Newman projection of the C-11–C-12 bond is shown above.

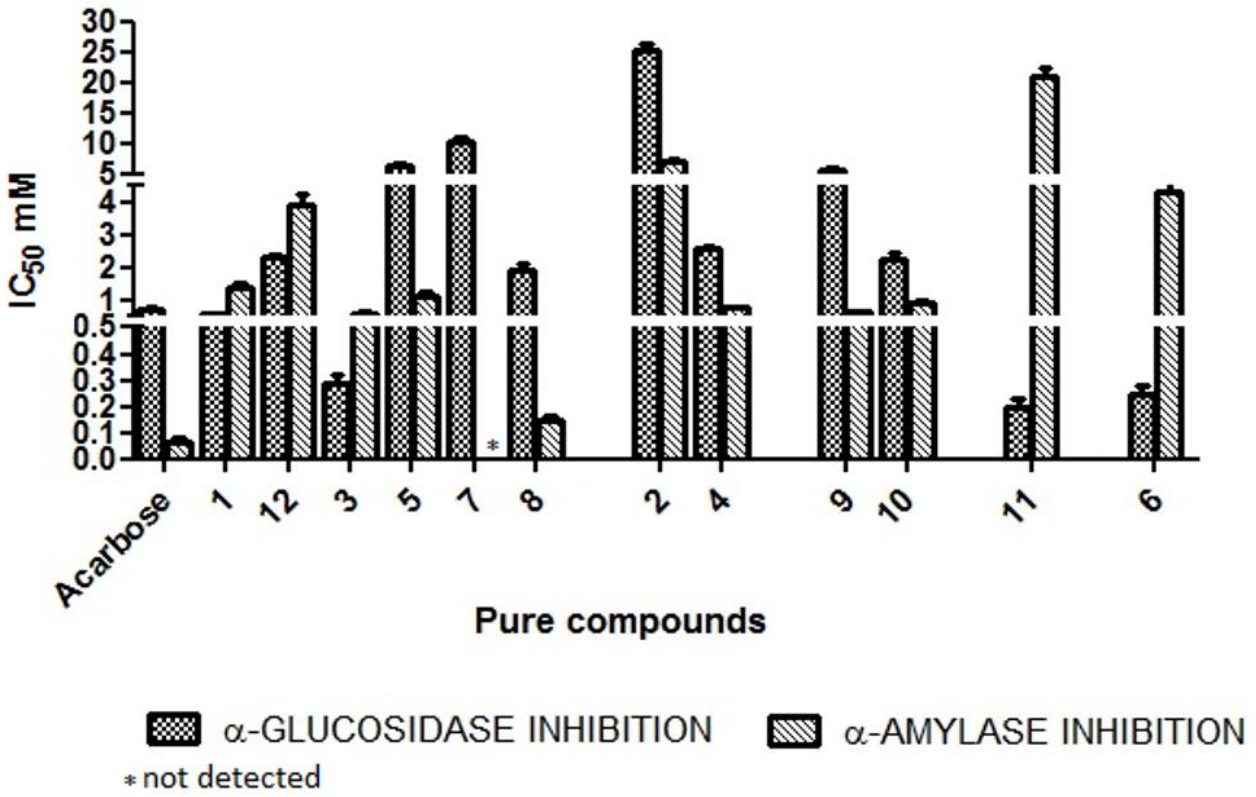

Figure 4. Inhibitory activities expressed as IC50 (mM) of acarbose and pure compounds from S. chamaedryoides (1–12) against α-amylase and α-glucosidase. The values are expressed as means ± SD of triplicate tests.

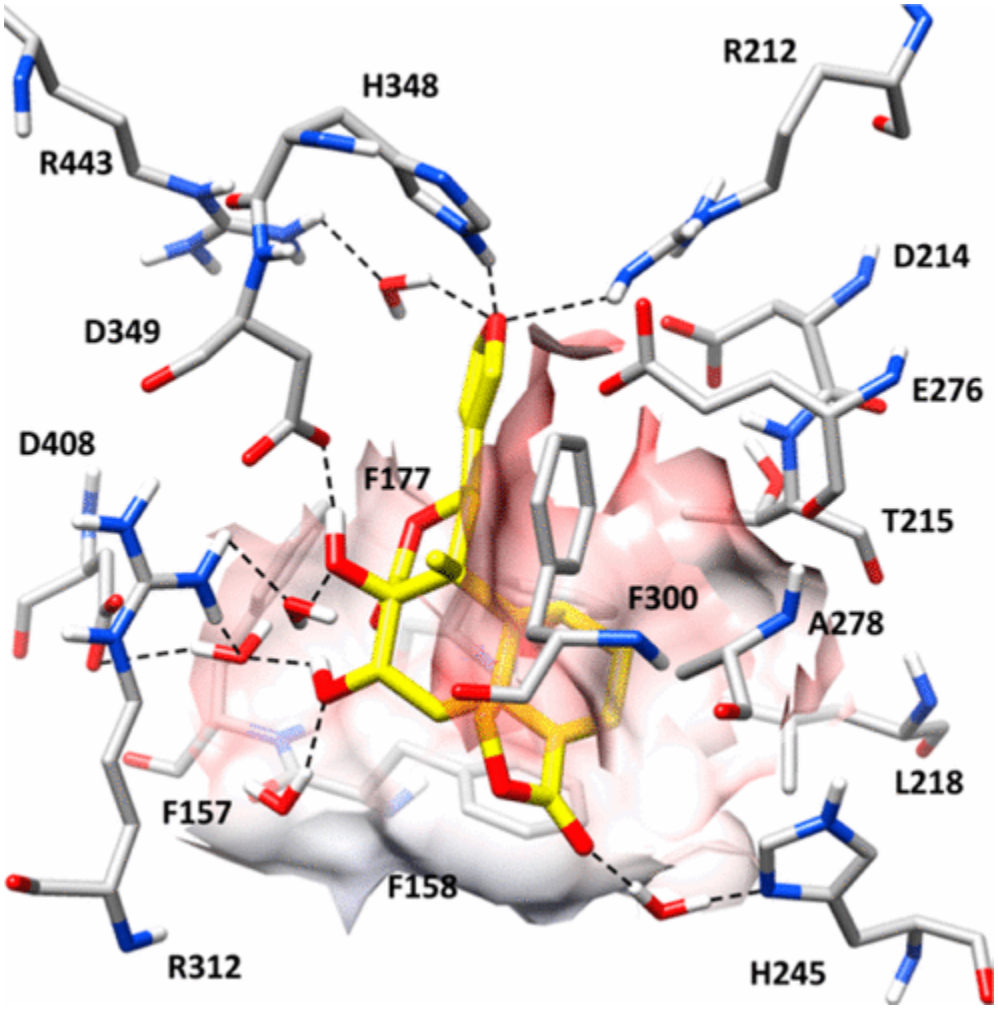

Figure 5. Minimized average structure of compound **3** bound to the catalytic site of α-1,4-glucosidase.